Neutron Diffraction Cryoporometry – a measurement technique for studying mesoporous materials and the phases of contained liquids and their crystalline forms.

J. Beau W. Webber [a,b,c], John C. Dore [b]

[a] *Institute of Petroleum Engineering, Heriot Watt, Edinburgh EH14 4AS, UK*
[b] *School of Physical Sciences, University of Kent, CT2 7NH, UK*
[c] *Lab-Tools Ltd., Canterbury Enterprise Hub, University of Kent, CT2 7NJ, UK*

Abstract

Neutron diffraction is a standard method for determining the structure of matter on an atomic scale; NMR cryoporometry is a recent widely-applicable technique for characterising structure on a 2nm to 2μm scale. An extension of these techniques is described, Neutron Diffraction Cryoporometry (NDC). The information from a set of neutron diffraction measurements of liquids and their crystalline forms in mesopores, as a function of temperature, is displayed as a cryoporometry graph. The data may then be conveniently interpreted using the Gibbs-Thomson relationship by analogy with the existing technique, NMR cryoporometry. Clear information is thus obtained on the relationship between phase and nano-structure, in a form well suited to further analysis. This method is applied to an equilibrium study of water/ice in SBA-15 templated silicas, as model nano- to meso-structured systems. The method described here uses global pattern matching (a one-dimensional morphing algorithm inside a linear least-squares fitting algorithm) applied to the full range of the diffraction data. This is a rapid method by comparison with the conventional method of fitting individual (overlapping) peaks, and has already led to NMR observations indicating plastic (rotator phase) ice in the same system.

Key words: confined geometry, phase-change, Gibbs-Thomson, neutron scattering, neutron diffraction, plastic ice, NMR, NMR relaxation, cryoporometry, DSC, thermoporosimetry, global fitting, pattern matching, morphing, porous silica.
PACS: 64.60.-i, 81.07.-b, 61.12.Ld, 61.18.Fs, 03.75.Hh, 05.70.Fh, 64.60.Qb, 64.70.Dv, 68.03.Cd, 68.08.-p, 82.56.Na, 82.56.Ub, 61.43.Gt, 61.46.+w, 82.60.Qr

Email address: `J.B.W.Webber@kent.ac.uk` (J. Beau W. Webber).

1   Introduction

There are a number of techniques for characterising structured matter at small length scales that employ thermodynamic protocols based on the Kelvin equation or the Gibbs-Thomson equation.

A formalism is applied that was first used with differential scanning calorimetry (DSC) thermoporosimetry (1; 2), and more recently with NMR cryoporometry (3; 4), whereby the melting behaviour of a liquid in nano- through meso- to micro-scale pores (2nm to 2μm) is interpreted using the Gibbs-Thomson relationship (5; 6; 7): this relationship states that the melting point depression of a small crystal of the liquid is inversely proportional to the size of the crystal.

This paper presents an extension of this formalism to neutron diffraction data, "Neutron Diffraction Cryoporometry", and discusses its application to a study of water/ice in a mesoporous silica. For all these techniques, a signal proportional to the quantity of each observed phase of the liquid/crystalline systems is plotted as a function of temperature, for cooling and/or warming temperature ramps. This information is then interpreted using the Gibbs-Thomson relationship, to give information on the structural features of the phases within the sample, as well as information on the confinement dimensions.

2   DSC Thermoporosimetry, NMR & Neutron Diffraction Cryoporometry.

2.1   The Gibbs-Thomson equation

The Gibbs-Thomson equation is the constant-pressure variant of a set of thermodynamic equations (5; 8), whereas the Kelvin equation (6, Eqn. 2, p. 450), (7, Eqn. 171, p. 163) is the constant temperature variant.

This behaviour is closely related to the capillary effect and both reflect the change in free energy caused by the curvature of an interfacial surface under tension (9; 10). Consequently, the Gibbs-Thomson equation for the melting point depression, ΔT_m, for a small isolated spherical crystal of diameter x may be written (2) as :-

$$\Delta T_m = T_m^\infty - T_m(x) = \frac{4\sigma_{cl}T_m^\infty}{x\Delta H_f \rho_s} \qquad (1)$$

where :

$$T_m^\infty \quad = \quad \text{normal melting point (i.e of a crystal of infinite size)},$$

$$T_m(x) \quad = \quad \text{melting point of crystals of diameter } x,$$

$$\sigma_{cl} \quad = \quad \text{surface energy at the crystalline-liquid interface},$$

$$\Delta H_f \quad = \quad \text{bulk enthalpy of fusion (per gram of material)},$$

$$\rho_s \quad = \quad \text{density of the solid}.$$

ΔT_m depends only on the properties of the liquid, its solid, and the interfacial interaction between these two states.

The presence of a confining geometry requires additional terms to be incorporated into the Kelvin and Gibbs-Thomson equations to accommodate the interaction between the adsorbate and the pore walls. For a crystal melting in a cylindrical pore the Gibbs-Thomson equation (1) becomes

$$\Delta T_m = T_m^\infty - T_m\left(x\right) = \frac{4\sigma_{cl}T_m^\infty}{x\Delta H_f\rho_s}\cos\left(\phi\right) \tag{2}$$

The contact angle is commonly assumed to be 0° in the liquid-vapour (Kelvin) case and 180° in the solid-liquid (Gibbs–Thomson) case (10; 2; 11; 12; 13). The $\cos(\phi)$ term also has a straightforward geometric interpretation since a spherical meniscus of radius r_1, in a cylindrical capillary of radius r, with an angle of contact ϕ, has $r = r_1 \cos(\phi)$ (10).

If, with suffixes l: liquid, s: solid, p: pore wall, we apply the Young equation $\sigma_{pl} = \sigma_{sl} \cdot \cos\left(\phi\right) + \sigma_{ps}$ and the Young-Dupré equation $W_{ps} = \sigma_{sl} + \sigma_{pl} - \sigma_{ps} =$ the reversible work required to separate unit area of the solid from the pore wall (9; 10), we obtain an expression for the contact angle :

$$\cos\left(\phi\right) = \frac{W_{ps}}{\sigma_{sl}} - 1 \tag{3}$$

The Gibbs-Thomson equation may also be written in a simpler form (3):-

$$\Delta T_m = \frac{k_{GT}}{x} \tag{4}$$

where x is a dimension that defines the effective size of the pore and k_{GT} is a constant that depends on the liquid, the pore geometry and the wetting nature of the pore walls.

More specifically,

$$\Delta T_m = \frac{k_{GT}}{x} = \frac{k_g \cdot k_s \cdot k_i}{x},\tag{5}$$

where, k_g is a geometric constant dependent on the interfacial shape (14), $k_s = \frac{T_m^\infty}{\Delta H_f \rho_s}$ is a constant specific to the solid crystal thermodynamic parameters, and $k_i = \sigma_{sl} - W_{ps}$ is a constant specific to the two inter-surface interaction terms of the crystal.

The conventional constant, "4", in the Gibbs-Thomson equation (eqn 2) is the manifestation of the k_g term, and is only appropriate to a hemispherical crystalline-liquid interface in cylindrical geometry. It is currently believed that the structural geometry factor k_g is a function of the pore surface to area ratio (14; 15). However there is still some current work relating to the exact nature of this relationship (16; 17).

Prior theoretical analysis (14; 15) suggests that for the melting event the theoretical ratio for $k_g^{sphere}/k_g^{cylinder}$ may be either 3/2 or 2, depending on the models used. In the experimental sections on calibration (section 3) and in both the NMR cryoporometry results (section 5) and the ND cryoporometry results (section 6) it appears that the measured ratio is close to 2, for agreement with gas adsorption results.

2.2 DSC Thermoporosimetry

Thermoporosimetry (1; 18; 2; 19; 20; 21) is an established technique, whereby thermal fluxes to or from a nanostructured liquid and its crystalline forms are monitored, while raising or lowering the temperature, so as to locate phase transitions as a function of temperature. These measurements may then be interpreted by the Gibbs-Thomson relationship to determine if the liquid is confined, and if so, to determine crystal/pore size distributions. Resolution of mono-modal distributions and precision of measured pore size are limited with this technique by the need to ramp the temperature at a sufficiently high rate so as to maintain measurable temperature fluxes.

2.3 NMR Cryoporometry

NMR Cryoporometry (3; 4) is a recent technique we have been developing (22; 23; 24; 25; 26; 27; 28; 29; 30; 14; 31; 32; 33), that makes use of the

Gibbs-Thomson relationship to deduce information regarding the pore size distributions in nano- to micro-structured materials - i.e. 2nm to 2μm.

A quantity of a liquid, such as water, is added to the mesoporous sample (more is added than is needed to fill the pores). On equilibration, the pores are filled leaving excess liquid on the external surfaces of the particulate grains. The sample is placed inside an NMR probe and is cooled until all the liquid is frozen. The sample is warmed gradually, at a controlled rate, while monitoring the amplitude of the NMR signal from the liquid (Figure 1). Due to the reorientational averaging from motion, the T_2 transverse relaxation time is much longer in liquids than in solids, providing a method of measuring the liquid quantity separately from that of the solid.

Thus the signal from brittle ice decays with a Gaussian free induction decay (FID) in about 10μs, while the exponential transverse relaxation time T_2 for water in meso-pores is typically of the order of 10ms. The application of an NMR "$90°$ - τ - $180°$ - τ - echo" pulse sequence enables the measurement of the liquid signal amplitude at a time 2τ when the brittle ice signal has decayed. Due to the decay of the liquid signal on a time-scale of T_2, for calibrated measurements, readings need to be made at more than one value of 2τ, to extrapolate to an effective liquid amplitude at $2\tau=0$ (28, Ch. 7.3.6, App. E). An NMR T_2 measurement is thus a sensitive technique for determining the quantity of melted liquid, deep inside the pores.

NMR cryoporometry measurements are static measurements of signal amplitude, and thus the temperature scanning may be done arbitrarily slowly (or even at a series of discrete temperatures, provided sufficient time is left for equilibration at each temperature.) Measuring the melting point, both of the liquid in the pores and of the bulk liquid, provides zero-order correction of the melting point depression for errors due to a finite temperature scanning rate. Making scans at more than one temperature allows for first-order correction to an effective zero temperature scanning rate.

2.4 Neutron Diffraction Cryoporometry

High-flux neutron diffractometers with multi-detectors covering a large range of scattering angles, such as D20 at Institute Laue-Langevin (34), can rapidly measure complete diffraction patterns simultaneously at good signal-to-noise ratio, enabling phase changes to be studied in detail as a function of temperature and time. The diffraction pattern measured at each temperature is plotted as a function of the scattering vector q. These may be analysed to obtain plots of the scattering intensities for the differing liquid and crystalline phases in the sample as a function of temperature, making it possible to per-

form cryoporometric measurements.

The particular advantage of using neutron diffraction cryoporometry, over DSC thermoporosimetry and NMR cryoporometry, is that the evolution of different crystalline phases with temperature may be assigned and plotted, in addition to that of the liquid phase. A prime strength of neutron diffraction cryoporometry is that the application of the Gibbs-Thomson equation may then be used to give structural and dimensional information complementary to that from the Debye-Scherrer relation, but potentially to larger structural dimensions. As well as determining if any particular phase of the crystalline/liquid system is confined or not, NDC can also measure pore size distributions, rather than just give a single estimate of crystal size.

The main difficulty in obtaining the scattering intensities needed for neutron diffraction cryoporometry, from the measured scattering data-set, for the various crystalline/liquid phases in the sample, is that the peaks from different phases frequently overlap. Some peaks (from structural disorder) may be very broad, with their true intensity obscured by Bragg peaks (whose measured intensities in turn are increased in in amplitude by this unknown amount). Furthermore, some Bragg peaks from different phases may be nearly coincident in q. In addition, thermal expansion of the sample results in the peak positions changing in q as the sample temperature changes.

2.4.1 Standard peak fitting techniques

Separation by individual peak fitting is possible, though a slow process. Initial linear fitting to peaks has been performed on some of the data, and is reported elsewhere (35). The results from this technique are discussed further in section 6.4. Multi-component non-linear fitting of overlapping peaks is proceeding (36; 37).

2.4.2 Global pattern matching

To analyse the diffraction data, a routine consisting of a one-dimensional morphing algorithm inside a linear least-squares fitting algorithm has been developed. Morphing is a common algorithm whereby a (typically 2D) structure is generated by interpolating or warping between two templates (38). A simple 1D-morphing algorithm, with a set of 1D templates corresponding to each of the phases identified in the measured data, is wrapped inside a standard linear least-squares fitting algorithm (39) so as to generate any arbitrary mixture of the templates, in such a way as to best match the measured 1D data.

Applying such an algorithm to the measured neutron scattering data generates a set of coefficients, as a function of temperature, whose amplitudes are

related to those of the quantities of each phase for which a template is provided. The least squares algorithm adjusts these coefficients so as to generate morphed curves that are the best match to the scattering data measured at each temperature. This is a rapid technique, both to implement, requiring only a few lines of code, and also to execute an analysis, the protocol being devised, the algorithm written and initial neutron diffraction cryoporometry graphs obtained, all within the same week as the measurement run. This speed of analysis makes neutron diffraction cryoporometry a viable and routine technique.

3 Calibration of the Gibbs-Thomson coefficient

DSC thermoporosimetry, NMR cryoporometry and ND cryoporometry are all secondary techniques, in that currently the thermodynamic coefficients of liquids are not known with sufficient precision to calculate Gibbs-Thomson coefficients directly from thermodynamic data, and they rely on other (primary) techniques for their pore-size calibration. To date, it has been usual to take a number of porous samples with different pore sizes as measured by gas adsorption and generate plots of measured melting point depressions against the inverse of these pore sizes, such that the slope gives the coefficient for a particular liquid (2; 40; 28; 29; 41; 42; 43).

There is significant evidence that in certain circumstances the melting point depression data shows a best fit when using $x - 2\varepsilon$ in the Gibbs-Thomson equation, rather than just x, where ε is a surface layer of adsorbate with modified molecular dynamics (44; 40; 41). The properties of this layer are further revealed by the results of these ND cryoporometry measurements, as discussed in sections 5 and 6.4, and by the subsequent NMR investigations (33; 45).

The effect of the geometry term k_g becomes evident if one compares NMR measurements of k_{GT} for the pore diameter made on sol-gel silicas (spherical pores, on average) $k_{GT}^{sol-gel} = 582$ {K.Å}, $\varepsilon = 0$Å, (28; 29; 43), with DSC measurements made on SBA-15 and MCM-41 silicas (cylindrical pores) : $k_{GT}^{cylinder}$ = 1040 ± 4 {K.Å}, $\varepsilon = 4$Å, (41), and these NDC and subsequent NMRC measurements made on SBA-15, for which : $k_{GT}^{cylinder} \sim 2$ x $k_{GT}^{sol-gel} = 1164 \pm 5$ {K.Å}, $\varepsilon \sim 2.5 \pm 1.5$ Å, (16). Within the scope of the remainder of this discussion on results from cylindrical mesopores, the latter value of $k_{GT}^{cylinder}$ is employed; given the current uncertainty in ε a value of zero is used. Thus these preliminary measurements are consistent with the analytic ratio

$$k_g^{sphere}/k_g^{cylinder} = 2 \qquad (6)$$

in agreement with some theoretical models, but not others (section 2.1). Further investigations are currently in progress (17).

4 Applications - the sample

To provide a clear indication of the effects of the Gibbs-Thomson relationship, a sample with a very narrow pore distribution was used in this study : SBA-15 templated silica - TLX-1-5 (F5), prepared at the Department of Chemistry, Technical University Berlin (41). This highly regular material has cylindrical pores on an hexagonal lattice, and was initially characterised by gas adsorption as having a pore diameter of 92 ± 5Å, on the basis of the Kelvin equation and the FHH equation for the thickness of the adsorbed film. Later measurement gave a value of 86 ± 5 Å, possibly reflecting an evolution with time. (35).

5 NMR Cryoporometry - an application

NMR cryoporometric measurements were made on a dedicated scanning NMR cryoporometer (28; 29). Various small ($\sim$ 30mg) samples of the SBA-15 templated silica TLX-1-5 (F5) were prepared in flame-sealed thin-walled 5mm O.D. NMR sample tubes. The pre-dried samples were slightly overfilled with distilled H_2O water (i.e. with excess bulk liquid around the grains), being weighed at each stage of the preparation. The samples were cooled in the NMR probe until all the liquid was frozen, and then measurements made while warming the sample on a slow linear warming ramp.

In Figure 1, for H_2O in this porous silica there is a clear melting process (D to C) associated with the melting of the ice in the pores, over a narrow temperature range, at a temperature well below the normal bulk melting point. There is then a plateau (C to B), followed by a further rise (B to A) at the normal melting point, to a new plateau, associated with the melting of the ice formed from excess bulk liquid outside the silica grains.

This technique may be used to determine accurately the total pore volume, using the ratio of the amplitudes of the two plateaux (B / A) and the known volume of liquid in the sample. Corrections must be made to compensate for the loss of signal amplitude due to the T_2 values of the liquids both inside and outside the pores (28; 29), and measurements at $2\tau = 1$, 2 and 4 ms enabled extrapolation to $2\tau = 0$.

On a warming ramp a melting phase transition (D – C) at $T_{mP} = T_m^\infty - \Delta T_{GT}$ is observed for the liquid in the pores and a further transition (B – A) at the
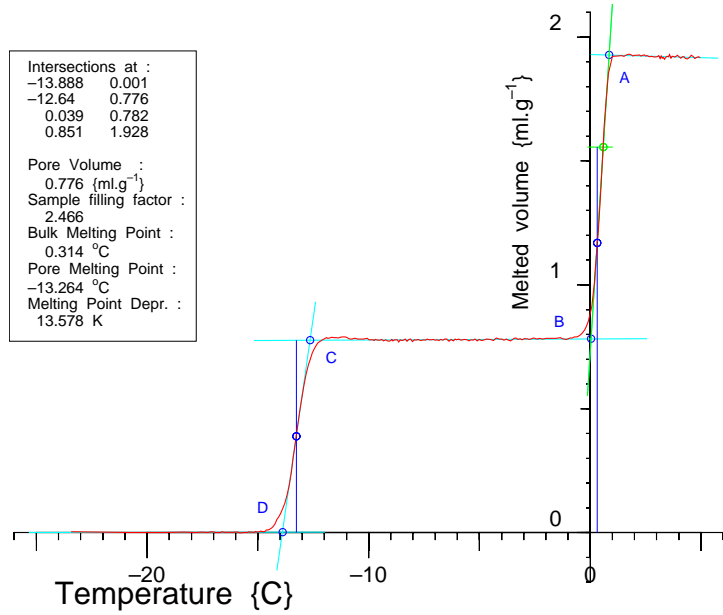
Fig. 1. NMR cryoporometric melting curve for H_2O in SBA-15 TLX-1-5 (F5) templated silica, at a warming rate of 0.05C°.min^{-1}.

normal melting point T_m^∞ for the bulk liquid around the porous grains. Having both a phase transition inside the pores and one in the bulk liquid enables the melting point depression to be measured with good accuracy, compensating for static temperature offsets in the apparatus and to zero order for warming-rate dependent offsets that occur when performing the measurement using a linear warming ramp. Warming rates used with this sample were 0.05, 0.1 and 0.2 K.min^{-1}, enabling first order corrections to be made to the melting point depression (28).

Application of the Gibbs-Thomson relationship, involving a differentiation and remapping (3), transforms the measured data Figure 1) to a pore size distribution (Figure 2).

The values obtained for a recent set of measurement on this sample of SBA-15 TLX-1-5 (F5) templated silica by NMR cryoporometry were : pore volume (water) = 1.11 ml.g^{-1} (corrected to 2τ =0), ΔT_{GT} = 13.6 ±0.1 C° (corrected to warming rate = 0) and pore diameter = 85.6 ±0.6 Å (median), 85.4 ±0.6 Å (peak) (corrected to warming rate = 0), assuming a cryoporometric constant $k_{GT}^{cylinder}$ = 2 x $k_{GT}^{sol-gel}$ = 1164 {K.Å}. See section 7 for a discussion of these results.
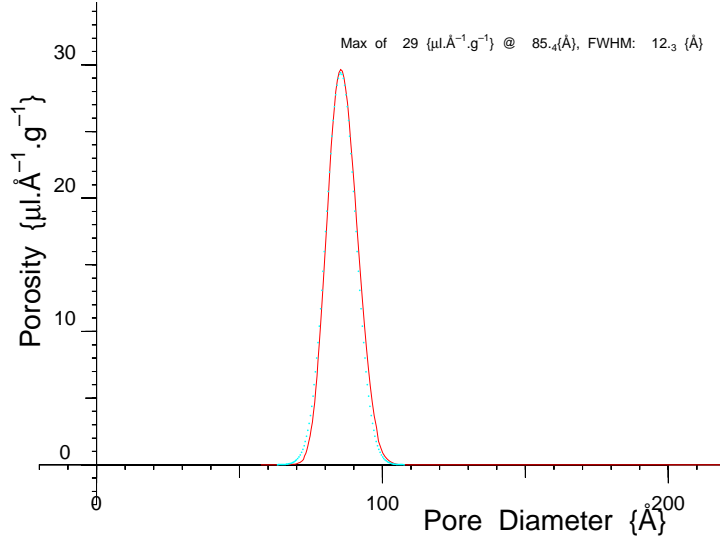
Max of 29 $\{\mu l.\text{Å}^{-1}.g^{-1}\}$ @ 85.4{Å}, FWHM: 12.3 {Å}

Fig. 2. Pore size distribution, for H_2O in SBA-15 (F5) templated silica, from NMR cryoporometry.

6 Neutron Diffraction Cryoporometry - an application

6.1 The experimental run

A set of over 1800 neutron diffraction datasets has been obtained using the D20 diffractometer, each covering the q range $0.30 \leq q \leq 5.06$ Å^{-1}, studying the behaviour of water/ice in SBA-15 templated silicas as a function of pore filling ratio and temperature, cooling and then warming. The most relevant of these for the purposes of this discussion is a set of 330 measurements made on the SBA-15 TLX-1-5 (F5) material, overfilled with D_2O (i.e. with excess bulk liquid around the grains), over the temperature cycle 300K to 181K to 300K, warming and cooling at 0.6K/min, and measuring each complete diffraction pattern with an averaging time of two minutes (46).

6.2 The data

Figure 3 shows a selection of the datasets, measured on the warming run, plotting every tenth diffraction curve. At the highest temperatures there is a broad liquid-water peak, at lower temperatures the signal shows the hexagonal ice melting to water, and at yet lower temperatures there is a complex inter-conversion between defective cubic ice, hexagonal ice and a 'water-like' component.

Neutron diffraction data from condensed matter is highly dependent on the phase of the material; in the present instant for scattering data from D_2O
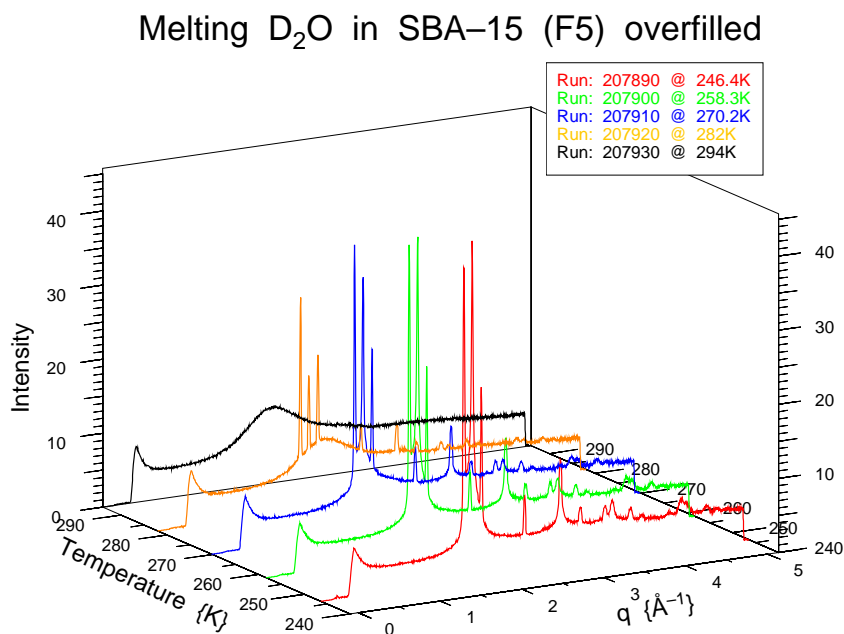
10

Fig. 3. Neutron diffraction curves for the melting of ice to water in overfilled SBA-15 (F5) templated silica. Scattering from the cryostat has been subtracted; that from the dry silica was subtracted at a later stage in the analysis.

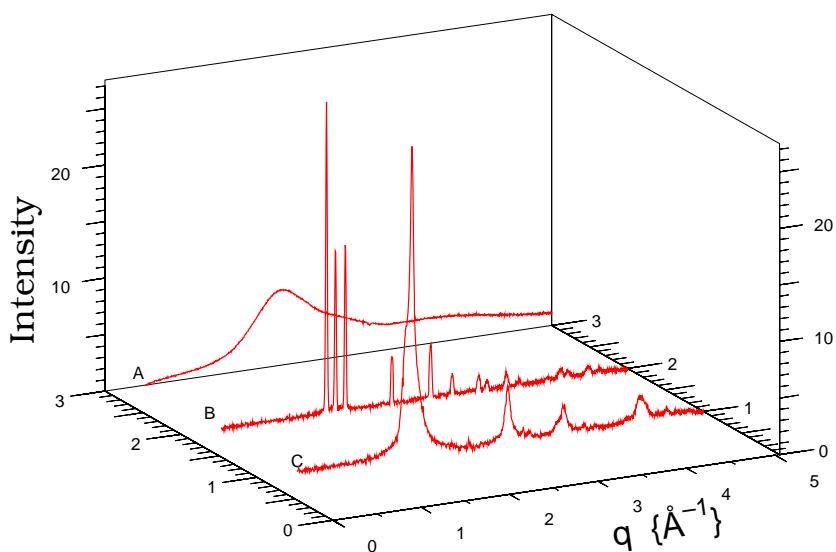**Three Templates for Neutron Diffraction Cryoporometry**

Fig. 4. Neutron diffraction curves for three ice/water phases: A) water, B) hexagonal ice, C) defective cubic ice.

(Figures 3, 4), liquid water shows as a broad first peak (294K, 4-A), hexagonal ice shows a sharp triplet of peaks (below 286K, 4-B), while cubic ice has a single main peak, but is actually found in a defective state giving a central peak with a shoulder (below 274K, 4-C). Studying these diffraction plots and quantifying this phase behaviour as a function of temperature is a process

11

that has been proceeding by conventional analysis (35; 36; 37). In all, there are up to 8 overlapping Bragg peaks (some themselves multi-component), plus the broad water peak, that are being quantified on each diffraction plot. In addition, it transpired that there is a broad disordered peak; this will be discussed later.

6.3 A rapid global fit Neutron Diffraction Cryoporometric analysis technique

An alternative fitting approach, that uses global fitting, is a two-stage one :

The first stage is to identify 'patterns', or 'templates', that represent the pure form of the scattering from the distinct phases to be identified, in this instance, water $P_w(q)$, hexagonal ice $P_h(q)$, and cubic ice $P_c(q)$; these profiles are shown in Figure 4. It should be noted that the $P_w(q)$ pattern was obtained from averaging a group of runs just above the melting temperature of all the ice, the $P_h(q)$ pattern was obtained by subtracting a suitably scaled copy (in intensity and q) of the $P_w(q)$ pattern from run 207920 (figure 3), and similarly the $P_c(q)$ pattern was obtained by subtracting suitably scaled copies (in intensity and q) of the $P_w(q)$ and $P_h(q)$ patterns, from run 207890. As part of the process, a routine was developed capable of automatically fitting and removing the q^{-4} SANS scattering tail (at low q) from each measurement in the data sets. The scattering from the dry silica was then subtracted from the total scattering in the data sets. This was thus used to help prepare the scattering templates for the three phases, over the q range of $0.45 \leq q \leq 5.05$ Å^{-1}.

For the second stage two alternative approaches have been developed : a) a simple linear algorithm, that is suitable for moderate temperature changes. If, however, the total temperature change is such that the diffraction peaks shift significantly in q over the measurement, due to thermal expansion or contraction, then a fitting technique must be used that allows for this. Thus, b), an extension of the basic algorithm has been developed to handle this shift in the peak positions.

6.3.1 Neutron Diffraction Cryoporometry – a) linear analysis

A least-squares fitting algorithm has been developed that can analyse the measured scattering curve at each temperature and quantify the scattering in terms of the amount of water, hexagonal ice and defective cubic ice that give rise to the data. Thus, at each temperature the measured scattering data set $I(T,q)$ is reduced to just four numbers, corresponding to the amplitudes of the three templates for the different phases $F_w(T), F_h(T), F_c(T)$ as well as the amplitude $C(T)$ of a spectrum that is constant in q (for the incoherent

12

scattering), such that the following sum provides the closest match to the measured data.

$$I(T,q) = F_w(T) \cdot P_w(q) + F_h(T) \cdot P_h(q) + F_c(T) \cdot P_c(q) + C(T) \cdot 1 \qquad (7)$$

A standard least-squares error-minimisation algorithm is used to find the four coefficients as a function of temperature - essentially this is just a 1D-morphing algorithm inside a least-squares fitting algorithm. For moderate temperature ranges a fast linear equation-solving algorithm may be employed. This was the first approach used; the above templates were extracted and an algorithm developed that evaluated the coefficients for the complete temperature run in just a few seconds (46).

This procedure allows the quantities of each phase present in part or all of the complete temperature cycle to be displayed on a single phase graph, of the same form as the NMR Cryoporometry graph in Figure 1. However it has the major advantage over standard NMR cryoporometry, in that in addition to a measurement of the water intensity, there are also curves delineating the melting of the crystalline phases. NMR can not easily discriminate between such brittle crystal phases.

However while appropriate for limited temperature ranges, a simple linear analysis is not sufficient for wide-ranging temperature runs, due to the temperature-dependent shift in q of the peak positions Q_0.

6.3.2   Neutron Diffraction Cryoporometry – b) non-linear analysis

An iterative non-linear algorithm may be employed (39), with a non-linear parameter for the shift $Q_0(q,T)$ of the peaks' positions in q with temperature T. For speed of convergence, each temperature step can use the coefficients from the previous temperature step as starting coefficients.

An alternative technique, that was actually employed, makes use of the fact that the dataset is based on measurements made with a linear temperature ramp : the fourth hexagonal ice peak was chosen from the hexagonal ice pattern (Trace B, Figure 4), as it is is not overlapped by a cubic ice peak, and a simple iterative fit was applied to this single peak for the complete dataset, to obtain $Q_0(q,T)$.

Figure 5 shows the measured $q(T)$ for the position of the maximum Q_0 of this Bragg peak, for a warming ramp, together with a simple cubic fit. It can be seen that the D20 instrument resolves the changes in q with a remarkable resolution. The fitted values were then used to scale the template data in q by an appropriate amount, at each temperature, before passing the modified
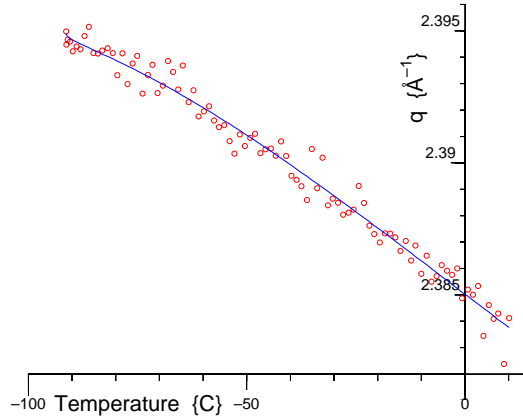
Fig. 5. Peak position $Q_0(q,T)$ for the 4th hexagonal ice peak, plotted as a function of temperature, together with a simple cubic fit.

template to the previous linear morphing routine.

There are a variety of methods of making this adjustment, including direct numerical interpolation or simple local spline/polynomial fits to the data that are then indexed at the modified q values. The method that was actually used was to globally fit a 200 part quintic piecewise-polynomial to each of the three templates, that could then, together with the modified q vector, be passed to a piecewise-polynomial reconstruction function, and thence to the morphing routine.

6.4 Neutron Diffraction Cryoporometry results and analysis

The results from the cryoporometry calculation (Figure 6), show three curves on a cooling ramp and three curves on a warming ramp; i.e. for each ramp there is a measure of the quantity for each of the water, hexagonal ice and cubic ice phases.

The hexagonal ice mostly melts at a temperature corresponding to the bulk melting point of D_2O. Thus, this hexagonal ice must be formed from the excess water outside the silica grains.

The defective cubic ice mostly melts to water with a temperature corresponding to a Gibbs-Thomson melting point depression appropriate to the pores – thus the defective cubic ice must be formed in the SBA pores.

Hence, this technique gives nano- to meso-structural information from neutron diffraction data. The alternative neutron technique of small-angle scattering techniques would not discriminate between the crystalline structures.

The use of the $q(T)$ scaling for the water and ice templates, as described in
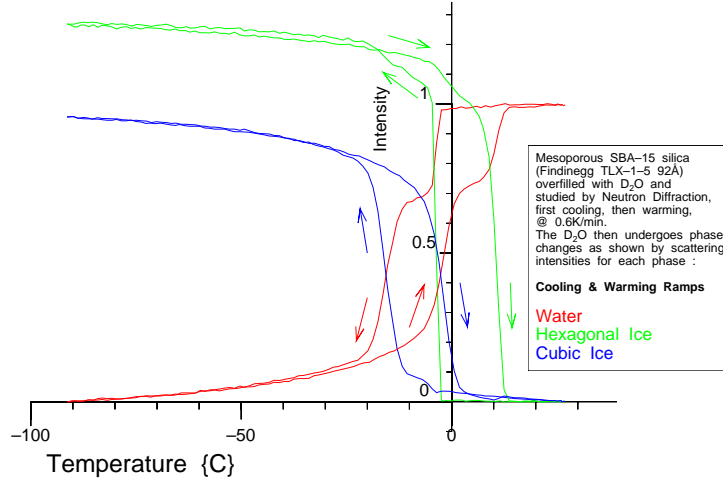
14

Fig. 6. Neutron diffraction cryoporometric curves for ice/water freezing and melting in overfilled SBA-15 (F5) templated silica with a nominal pore diameter of 86Å - using the nonlinear algorithm.

section 6.3.2, improves the extraction of amplitudes of the hexagonal and cubic ice components over the full temperature range of the measurement and Figure 6 shows good agreement with the results from the conventional analysis (35, Fig. 9) - this presentation was delayed until this comparison could be made.
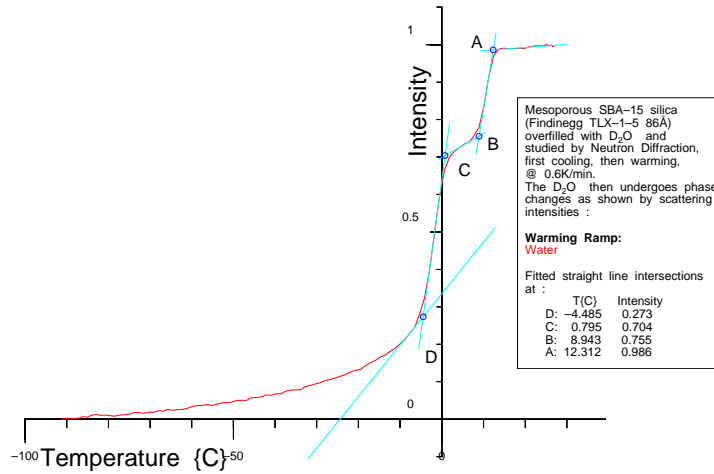

Fig. 7. Neutron Diffraction Cryoporometry curves for water melting in overfilled SBA-15 (F5) templated silica with a nominal pore diameter of 86Å - nonlinear algorithm.

The segments of the measured "water-melting" curve (Figure 7), may be fitted linearly to extract robust data, as per Figure 1. Information is obtained for the large step, due to the melting of the cubic ice in the pore with a Gibbs-Thomson melting point depression, as well as for the smaller step due to the melting of the hexagonal ice around the grains. The difference between the medians of these temperature steps gives a value of $\Delta T_{GT} = 12.5$ C°, and the ratio of the amplitudes a filling factor $f = 1.31 \pm 0.05$. If a Gibbs-Thomson coefficient $k_{GT}^{cylinder} = 2 \times k_{GT}^{sol-gel} = 1164$ {K.Å} is used, then a measurement

15

of pore diameter = 93.3 ±6.0 Å (median) is obtained. See section 7 for a discussion of these results.

In addition, however, there appears to be a large 'water-like' signal at temperatures below that at which most of the cubic ice melts; this contribution has a significant component well below -50C, extending down to ∼ -80C. While this component is clearly disordered, like water (and hence is best fitted by the water template), examination of the scattering data shows a clear distinction. It is likely that this component is a form of amorphous ice, and these NDC measurements have led to NMR relaxation measurements being made to study the dynamics of this component. These measurements indicate the presence of ice in a plastic or rotationally mobile state. These measurements and conclusions are discussed in detail elsewhere : (35; 33; 45).

Thus NDC can be seen to be a valuable technique for spatially localising the phases of an imbibed liquid and their crystalline forms (within or outside the pores of a mesoporous system), just based on the inspection of the freezing/melting curves. In addition, pore-size distributions can be obtained - not as yet with the resolution of figure 2, which has been obtained using a dedicated NMR cryoporometer with well over a decade of optimisation. The neutron diffraction cryoporometry data in figure 6 was a first measurement using a standard 6mm diameter sample can and conventional 'orange cryostat' arrangement for the D20 instrument, and making additional use of data obtained for a conventional diffraction measurement. The degradation this causes to both the pore-size resolution (Gaussian σ) of the measurement and the accuracy of the measured pore diameter are discussed in more detail in section 7. However use can be made of the fact that the step in the melting curve due to the melting of the bulk liquid encodes the "instrument resolution function" - in an ideal measurement it would be a Heaviside step function. The measured sigmoidal function for this bulk step has thus been used to deconvolve the broader sigmoidal step function for the pore melting event. The bulk melting step has been approximated by the integral of a Gaussian, to obtain an instrument function, but no particular function has been assumed for the pore-size distribution.

Figure 8 shows the pore size distribution calculated from the water melting curve, and with such a deconvolution applied. The cryoporometric constant applied is again $k_{GT}^{cylinder} = 2 \text{ x } k_{GT}^{sol-gel} = 1164$ {K.Å}, and a pore diameter of 91.9 ±6.0 Å (peak) is obtained; this result is discussed further in section 7.
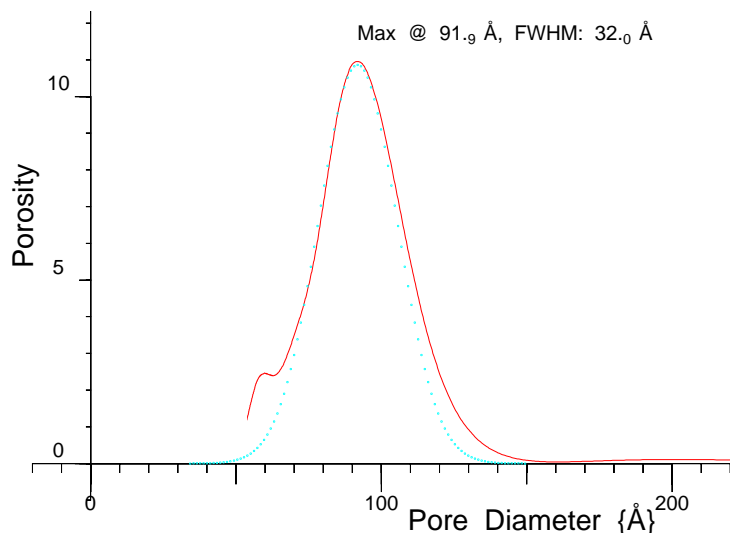
Fig. 8. Pore size distribution for D_2O in SBA-15 (F5) silica, from Neutron Diffraction Cryoporometry, after deconvolution with the instrument function.

7 Comparative Error Analysis

There are a number of possible sources of error in thermoporosimetry / cryoporometry measurements. There may be errors in temperature measurement, in amplitude measurement, in phase assignment and, most significantly, there may be systematic errors in the constant k_{GT}, particularly arising from an inappropriate dimensional term k_g. In Table 1, results are compared for different thermodynamic techniques : gas adsorption on the basis of the Kelvin equation and the Frenkel-Halsey-Hill (FHH) equation for the thickness of the adsorbed film, for the three thermoporosimetry/cryoporometry techniques, and for two methods of obtaining neutron diffraction cryoporometry graphs.

Firstly, a significant feature, is that all these techniques are most conveniently performed using a scanning protocol with continual temperature change ramps. The error in measured temperature that this causes is then a function of the total sample thermal-mass, the warming rate and the the distance of the temperature measuring device from the active volume of the sample. This process may readily be modeled as a first-order filter, either algebraically or numerically (28).

DSC relies on measuring transient heat flows due to the phase changes, and thus the warming rate must be such as to obtain measurable heat flows from the phase transitions. Since NMR and neutron scattering make static measurement of the phase quantity, the warming rate can be arbitrarily slowed, to improve resolution and/or the signal-to-noise ratio. A measure of the error due to scanning may be directly determined from the slope of the melting curve for the melting of the bulk liquid (see Figures 1, 7), and such a zero

17

Results and Error Comparisons for different thermodynamic techniques.

	Measured SBA-15 (F5) Pore Diameter				
	GA	DSC	NMRC	NDC (peak)	NDC (global)
median {Å} :	86.0 ±5	84.0 ±1.5	85.6 ±0.6	[nca]	93.3 ±6
peak {Å} :	[nca]	83.0 ±3	85.4 ±0.6	[nca]	91.9 ±6

	Scanning Thermal Broadening			
	DSC	NMRC		NDC
Sample Mass {mg} :	∼10	∼30		∼300
Warming Rate {K.min^{-1}} :	∼2	∼0.05		∼0.5
Broadening {arb.} :	∼20	∼1.5		∼150

	Fractional Amplitude % RMS Noise			
	DSC	NMRC	NDC (peak)	NDC (global)
Hexagonal Ice :	[nm]	[nm]	0.9%	0.2%
Cubic Ice :	[nm]	[nm]	0.9%	0.2%
Water :	0.005%	0.4%	[nca]	0.1%

Table 1
Measurement comparisons for different thermodynamic techniques and parameters, where available : Gas Adsorption, DSC Thermoporosimetry, NMR Cryoporometry, ND Cryoporometry (peak-fitting), ND Cryoporometry (global-fitting).
For pore diameter calculations using the Gibbs-Thomson equation :
$$k_{GT}^{cylinder} = 1164 \ \{K.Å\} = 2 \ k_{GT}^{sol-gel} \ (\text{section 3}).$$
[nm] : not measurable.   [nca] : not currently analysed.

order correction has been applied to the DSC, NMRC and NDC median measurements, giving an approximately factor of 10 reduction in the error due to finite scanning rate, and partially applied to the peak-fitting measurements. In addition, with the NMRC median data, measurements at three different warming rates has enabled an extrapolation to zero warming rate.

Table 1 shows that the typical sample masses and easily accessible warming rates for the three techniques imply that NMR can be expected to have the best thermal and hence best spatial resolution of Gaussian σ, then DSC, with ND cryoporometry being the worst. However, the ability of ND cryoporometry to distinguish and resolve the signals from the crystalline phases, in a way that DSC and NMR can not, is far more significant.

Table 1 further shows that the pore diameters as measured by neutron diffraction cryoporometry (from both the medians of the melting temperature steps

and the peak of the pore distribution) agree well with those measured by NMR and DSC. The difference between NMR and neutron diffraction may possibly be due to a difference in the cryoporometric constants of H_2O and D_2O, but our first assumption must be that it is an instrumental one relating to the different thermal broadenings from the scanning protocols.

The fractional signal-to-noise ratio is measured for the pore plateaux where possible, and the maximum plateaux otherwise, and is obtained by fitting a low order polynomial to the plateau, checking that the residuals have the characteristics of random noise, calculating the rms amplitude of these residuals, and dividing by the average of the amplitude. The signal-to-noise ratio from the global fitting technique is significantly better than that from the peak fitting technique, and for the water melting curve is also better than that from NMR. For the DSC measurement, to compare the noise one needs to first integrate the data (which acts to reduce the noise); the residuals for these data are characterised by small oscillations with periods of about 1K and 3K and give by far the best of the signal-to-noise ratios. The crucial point however is that the NDC technique is the only one that is capable of resolving separate cryoporometry curves for the hexagonal and cubic ice components.

8 Future Developments

Figure 6 shows that that the traces are not normalised, There are good reasons that they should not be, as the traces are defined to represent the quantities of each phase. However in the existing algorithm, unity amplitude just corresponds to that of the patterns that we chose for templates. Further work needs to be performed to calibrate the system in terms of grams of D_2O for all the phases, and to handle the incoherent scattering in a more faithful manner. Further, there is an interest in generating a template for the disordered/amorphous ice component, to extract data for this separately from the water component.

A clear possibility for the future is to sacrifice some of the excellent signal-to-noise ratio offered by the global fitting technique, and, by reducing the mass of the sample, to obtain a more rapid thermal response and hence a better spatial resolution. This is currently being tested with NMR cryoporometry as a way of reducing total measurement time while obtaining improved resolution of the phase transitions. The limited beam-time access for instruments such as D20 means that the development of a sample can optimised for rapid NDC measurements is an important step if NDC is to be a routine technique,

9   Summary

The technique of Thermoporosimetry/Cryoporometry has been successfully adapted from DSC and NMR and applied to neutron diffraction data, using the global fitting of template curves to the measured data. The interpretation of phase information using the Gibbs-Thomson relationship is thus applied to a further measuring technique.

We have shown that, by applying Neutron Diffraction Cryoporometry, clear information has been obtained on the nano- to meso-structural location of multiple inter-converting phases in a form well suited to further analysis.

This form of analysis and presentation of the data has lead to the observation of a disordered component that NMR relaxation has indicated is ice in a plastic or rotationally mobile form (33; 45).

10   Acknowledgments

11   Appendix: Neutron Diffraction Cryoporometry Algorithm

To decompose a diffraction curve at a particular temperature, it is first necessary to prepare pure examples of each of the diffraction curves from the three phases (water, hexagonal ice, defective cubic ice, Figure 4).

The algorithm is expressed in the array manipulation language Apl :

A four column data-set Gjn is generated from the three $Templates(q, intensity)$:

$$Gjn \leftarrow (Cub[;2], (Hex[;2], [1.5]Water[;2])), 1$$

A simple 1-D morphing routine for this data-set is then wrapped inside a standard fast linear least-squares fitting algorithm, based on an equation solving routine:

For two column $Data$ (q, $intensity$), with a measurement set for these results over the temperature cycle $300K \rightarrow 181K \rightarrow 300K$:

$$Coefts \leftarrow (Gjn + . \times \ 0 \ 1 \downarrow Data) \boxdot Gjn + . \times \lozenge Gjn$$

where $\boxdot$ is the Apl matrix equation solving primitive, $+ . \times$ represents a conventional matrix inner product (or "matrix multiply") and $\lozenge$ transposes the matrix. $0 \ 1 \downarrow Data$ just selects the $intensity$ column of $Data$.

Thus the diffraction curves are fitted, so that the data set $I(q)$ at each temperature is reduced to four numbers, the amplitudes of the three phases and a constant, such that the scaled sum of the templates forms the best-fit match to the measured curve. This method appears to be more robust than individual peak fitting of overlapping peaks, and gives a better signal-to noise ratio (table 1).

It should be noted that the quantity denoted by a scattering feature is related to the integral of that feature. In the case of this algorithm, the structure and width of the feature is denoted by the example pattern being used, which remains constant. This thus gives a measure of the quantity of each component by determining the amplitude coefficient for each of the patterns, as each of these have a fixed characteristic integral.

A recent (2.5GHz) PC performs the linear transformation for the temperature cycle of 330 scattering curves in about five seconds. Including the Gaussian pre-fitting of one hexagonal ice peak for the warming scattering curves, to obtain the changes in q due to thermal expansion and contraction, slows the total analysis time down to about 50s but this is still very acceptable compared with the many stages of analysis needed for an individual peak fitting approach.

The existing algorithms are implemented in the array manipulation language Apl, using MicroApl's $APLX$ for MS Windows, PPC and Linux (47), but can readily be translated into C using $apl2c$ (48). Implementation in other languages with array manipulation capabilities and a linear equation solver should be straightforward.

References

[1] M. Brun, A. Lallemand, J.-F. Quinson, C. Eyraud, A new method for the simultaneous determination of the sizeand the shape of pores: The thermoporometry, Thermochimica Acta 21 (1977) 59–88.

[2] C. Jackson, G. McKenna, The melting behavior of organic materials confined in porous solids, J. Chem. Phys. 93 (12) (1990) 9002–9011.

[3] J. Strange, M. Rahman, E. Smith, Characterisation of porous solids by NMR, Phys. Rev. Letts. 71 (21) (1993) 3589–3591.

[4] J. Strange, Cryoporometry: A new NMR method for characterising porous media, Nondestr. Test. Eval. 11 (1994) 261–271.

[5] J. Gibbs, The scientific papers of J.Willward Gibbs, New Dover Edition, Vol. 1: Thermodynamics, Dover Publications, Inc., Constable and Co., New York, London, 1906 reprinted 1961.

[6] W. Thomson, On the equilibrium of vapour at a curved surface of liquid, Phil. Mag. 42 (282) (1871) 448–452.

[7] J. Thomson, Application of dynamics to Physics and Chemistry, Macmillan & Co, London, 1888.

[8] J. Gibbs, Collected Works, Longmans, Green and Co., New York, 1928.

[9] R. Defay, I. Prigogine, A. Bellemans, D. Everett, Surface tension and adsorption, english Edition, Longmans, Green & Co Ltd., London, 1951, 1966.

[10] S. Gregg, K. Sing, Adsorption, Surface Area and Porosity, 2nd Edition, Academic Press, London, 1967.

[11] T. Young, An essay on the cohesion of fluids, in: G. Peacock (Ed.), Miscellaneous Works of the late Thomas Young, Vol. 1, John Murray, Albemarle Street, London, 1855, Ch. XIX, pp. 418–453.

[12] J. L. Tell, H. J. Maris, Specific heats of hydrogen, deuterium, and neon in porous vycor glass, Phys. Rev. B 28 (9) (1983) 5122–5125.

[13] T. Martin, B. Lefevre, D. Brunel, A. Galarnea, F. D. Renz, F. Fajul, P. F. Gobi, J. F. Quinson, G. Vigier, Dissipative water intrusion in hydrophobic mcm-41 type materials, Chem. Commun. 1 (2002) 24–25.

[14] J. Webber, A generalisation of the thermoporisimetry Gibbs-Thomson equation for arbitrary pore geometry, Magn. Reson. Imaging 21 (3-4) (2003) 428.
URL http://dx.doi.org/10.1016/S0730-725X(03)00172-3

[15] O. Petrov, I. Furo, Curvature-dependent metastability of the solid phase and the freezing-melting hysteresis in pores, Physical Review E 73 (1) (2006) 7.

[16] J. Webber, J. Strange, J. Dore, The characterisation of sol-gel and templated porous silicas. In preparation.

[17] J. Webber, A generalisation of the thermoporisimetry Gibbs-Thomson equation for arbitrary pore geometry. In preparation.

[18] C. Eyraus, J. Quinson, M. Brun, Characterisation of porous solids, Elsevier, Amsterdam, 1988.

[19] C. Jallut, J. Lenoir, C. Bardot, C. Eyraud, Thermoporometry. modelling and simulation of a mesoporous solid, Journal of Membrane Science 68 (1992) 271–282.

[20] K. Ishikiriyama, M. Todoki, K. Motomura, Pore size distribution(PSD) measurements of silica gels by means of differential scanning calorimetry. I: Optimization for determination of PSD, Journal of colloid and interface science 171 (1) (1995) 92–102.

[21] K. Ishikiriyama, M. Todoki, Pore size distribution measurements of silica gels by means of differential scanning calorimetry. II: Thermoporosimetry, Journal of colloid and interface science 171 (1) (1995) 103–111.

[22] S. Alnaimi, J. Strange, E. Smith, The characterisation of porous solids by NMR, Magnetic Resonance Imaging 12 (2) (1994) 257–259.

[23] J. Strange, J. Webber, Characterization of porous solids by NMR, in: 12th Specialized Colloque Ampere, Corfu., Athens, 1995.

[24] J. Strange, J. Webber, S. Schmidt, Pore-size distributions mapping, Magn. Reson. Imag. 14 (7/8) (1996) 803–805.
URL http://dx.doi.org/10.1016/S0730-725X(96)00167-1

[25] J. Strange, J. Webber, Multidimensionally resolved pore size distributions, Appl. Magn. Reson. 12 (2-3) (1997) 231–245.

[26] J. Strange, J. Webber, Spatially resolved pore size distributions by NMR, Meas. Sci. Technol. 8 (5) (1997) 555–561.
URL http://www.iop.org/EJ/abstract/0957-0233/8/5/015

[27] S. Alnaimi, The characterisation of porous media by NMR, Phd, Physics, University of Kent at Canterbury, UK. (1994).

[28] J. Webber, The characterisation of porous media, Phd, Physics, University of Kent at Canterbury, UK. (2000).
URL http://www.kent.ac.uk/physical-sciences/publications/theses/jbww.html

[29] J. Webber, J. Strange, J. Dore, An evaluation of NMR cryoporometry, density measurement and neutron scattering methods of pore characterisation, Mag. Res. Imag. 19 (3-4) (2001) 395–399.
URL http://dx.doi.org/10.1016/S0730-725X(01)00255-7

[30] J. Strange, J. Mitchell, J. Webber, Pore surface exploration by NMR, Magn. Reson. Imaging 21 (3-4) (2003) 221–226.
URL http://dx.doi.org/10.1016/S0730-725X(03)00128-0

[31] S. Alnaimi, J. Mitchell, J. Strange, J. Webber, Binary liquid mixtures in porous solids, J. Chem. Phys. 120 (5) (2004) 2075–2077.
URL http://dx.doi.org/10.1063/1.1643730

[32] B. Webber, J. Dore, Structural and dynamic studies of water in mesoporous silicas using neutron scattering and nuclear magnetic resonance, J. Phys.: Condens. Matter 16 (Special Issue: Water in Confined Geometry) (2004) S5449–S5470.
URL http://stacks.iop.org/JPhysCM/16/S5449

[33] J. B. W. Webber, R. Anderson, J. H. Strange, B. Tohidi, Clathrate formation and dissociation in vapour/water/ice/hydrate systems in SBA-15, sol-gel and cpg porous media, as probed by NMR relaxation, novel

protocol NMR cryoporometry, neutron scattering and ab-initio quantum-mechanical molecular dynamics simulation., Magn. Reson. Imaging 25 (4) (2007) 533–536.
URL http://dx.doi.org/doi:10.1016/j.mri.2006.11.022

[34] T. Hansen, the D20 instrument description. (2004,2007).
URL http://whisky.ill.fr/YellowBook/D20/

[35] E. Liu, J. C. Dore, J. B. W. Webber, D. Khushalani, S. Jähnert, G. H. Findenegg, T. Hansen, Neutron diffraction and NMR relaxation studies of structural variation and phase transformations for water/ice in SBA-15 silica: I. the over-filled case, J. Phys.: Condens. Matter 18 (44) (2006) 10009–10028.
URL http://stacks.iop.org/0953-8984/18/10009

[36] J. Seyed-Yazdi, J. Dore, J. Webber, G. Findenegg, T. Hansen, Structural characterisation of water and ice in mesoporous SBA-15 silicas 2: The 'almost-filled' case for 86 å pore diameter.

[37] J. Seyed-Yazdi, H. Farman, J. Dore, J. Webber, G. Findenegg, Structural characterisation of water/ice formation in SBA-15 - 3: The triplet profile.

[38] Wikipedia, Morphing, Web (1990-2006).
URL http://en.wikipedia.org/wiki/Morphing

[39] W. Evans, Advanced Numerical Techniques, University of Kent, Canterbury, UK, 1997 - 2005.

[40] E. Hansen, M. Stocker, R. Schmidt, Low-temperature phase transition of water confined in mesopores probed by NMR. influence on pore size distribution., J. Phys. Chem. US 100 (6) (1996) 2195–2200.

[41] A. Schreiber, I. Ketelsen, G. Findenegg, Melting and freezing of water in ordered mesoporous silica materials, Physical Chemistry Chemical Physics 3 (7) (2001) 1185–1195.

[42] J. Dore, B. Webber, J. Strange, H. Farman, M. Descamps, L. Carpentier, Phase transformations for cyclohexane in mesoporous silicas, Physica A 333 (2004) 10–16.
URL http://dx.doi.org/10.1016/j.physa.2003.09.043

[43] J. Dore, J. Webber, J. Strange, Characterisation of porous solids using small-angle scattering and NMR cryoporometry, Colloids and Surfaces A-Physicochemical and Engineering Aspects 241 (1-3) (2004) 191–200.
URL http://dx.doi.org/10.1016/j.colsurfa.2004.04.005

[44] J. Strange, J. Webber, Characterisation of porous solids by NMR, in: 12th Specialised Colloque Ampere, Corfu, 1995.

[45] J. B. W. Webber, J. C. Dore, J. H. Strange, R. Anderson, B. Tohidi., Plastic ice in confined geometry: The evidence from neutron diffraction and NMR relaxation., J. Phys.: Condens. Matter 19 (2007) 415117 (12pp).

[46] J. Dore, J. Webber, ILL experimental report 5-24-184. (2003).
URL http://club.ill.fr/cv/servlet/ReportFind

[47] R. Nabavi, micoApl's AplX interpreter. (2001-2007).
URL http://www.microapl.co.uk/APL/

[48] T. Budd, S. Sirlin, B. Webber, the APL c compiler project. (1988-2007).

URL `http://home.earthlink.net/ swsirlin/aplcc.html`